Nitrogen Embedding Enhances Stability and Activity of Single-Atom Motifs of MXenes under Anodic Polarization

Ling Meng,[a,b] Samad Razzaq,[c] Diwakar Singh,[c] Francesc Viñes,[a,*] Francesc Illas,[a]

Kai S. Exner[c,d,*]

[a] *Departament de Ciència de Materials i Química Física & Institut de Química Teòrica i Computacional (IQTCUB), Universitat de Barcelona, c/ Martí i Franquès 1, 08028 Barcelona, Spain.*

[b] *State Key Laboratory of Chemical Resource Engineering, Beijing Engineering Center for Hierarchical Catalysts, College of Chemistry, Beijing University of Chemical Technology, Beijing 100029, China*

[c] *Faculty of Chemistry, Theoretical Catalysis and Electrochemistry, University of Duisburg-Essen, Essen 45141, Germany.*

[d] *Cluster of Excellence RESOLV, Bochum 44801, Germany; Center for Nanointegration (CENIDE) Duisburg- Essen, Duisburg 47057, Germany.*

* Corresponding authors: francesc.vines@ub.edu; kai.exner@uni-due.de

Table S1. Summary of the nitrogen doping thermodynamic feasibility of SAC-like MXenes, 3O*-M_{SAC}-*O, of M_2X_1O MXene (M = Cr, Fe, Hf, Mo, Nb, Ta, Ti, V, W, and Zr) using gas-phase DFT calculations. ΔG is the Gibbs free energy of the nitrogen doping process (*cf.* Eq. (1)), and U_{eq} denotes the equilibrium potential of nitrogen doping process relative to the SHE.

M_2C_1O	**ΔG / eV**	**U_{eq} / V**	**M_2N_1O**	**ΔG / eV**	**U_{eq} / V**
Cr_2C	3.32	1.11	Cr_2N	3.65	1.22
Fe_2C	2.34	0.78	—	—	—
Hf_2C	4.24	1.41	Hf_2N	5.28	1.76
Mo_2C	2.28	0.76	Mo_2N	1.44	0.48
Nb_2C	4.18	1.39	Nb_2N	4.12	1.37
Ta_2C	3.70	1.23	Ta_2N	3.41	1.14
Ti_2C	4.79	1.60	Ti_2N	5.34	1.78
V_2C	4.44	1.48	V_2N	3.31	1.10
W_2C	0.07	0.02	W_2N	0.40	0.13
Zr_2C	5.07	1.69	Zr_2N	5.66	1.89

Table S2. Summary of the nitrogen doping thermodynamic feasibility of SAC-like MXenes, 3O*-M_{SAC}-*O, of M_3X_2O MXene (M = Cr, Hf, Mo, Nb, Ta, Ti, V, W, and Zr) using gas-phase DFT calculations. ΔG is the Gibbs free energy of the nitrogen doping process (*cf.* Eq. (1)), and U_{eq} denotes the equilibrium potential of nitrogen doping process relative to the SHE.

M_3C_2O	**ΔG / eV**	**U_{eq} / V**	**M_3N_2O**	**ΔG / eV**	**U_{eq} / V**
—	—	—	Cr_3N_2	3.40	1.13
Hf_3C_2	6.70	2.23	Hf_3N_2	2.82	0.94
Mo_3C_2	2.24	0.75	Mo_3N_2	1.77	0.59
Nb_3C_2	2.64	0.88	Nb_3N_2	2.41	0.80
Ta_3C_2	1.75	0.58	Ta_3N_2	5.29	1.76
Ti_3C_2	6.03	2.01	Ti_3N_2	4.14	1.38
V_3C_2	3.62	1.21	V_3N_2	2.56	0.85
W_3C_2	1.69	0.56	W_3N_2	0.89	0.30
Zr_3C_2	6.71	2.24	Zr_3N_2	3.59	1.20

Table S3. Summary of the nitrogen doping thermodynamic feasibility of SAC-like MXenes, 3O*-M_{SAC}-*O, of M_4X_3O MXene (M = Cr, Fe, Hf, Mo, Nb, Ta, Ti, V, W, and Zr) using gas-phase DFT calculations. ΔG is the Gibbs free energy of the nitrogen doping process (*cf.* Eq. (1)), and U_{eq} denotes the equilibrium potential of nitrogen doping process relative to the SHE.

M_4C_3O	**ΔG / eV**	**U_{eq} / V**	**M_4N_3O**	**ΔG / eV**	**U_{eq} / V**
—	—	—	Cr_4N_3	3.54	1.18
Hf_4C_3	7.40	2.47	Hf_4N_3	4.06	1.35
Mo_4C_3	2.25	0.75	Mo_4N_3	1.80	0.60
Nb_4C_3	3.47	1.16	Nb_4N_3	2.27	0.76
Ta_4C_3	2.74	0.91	Ta_4N_3	1.30	0.43
Ti_4C_3	6.72	2.24	Ti_4N_3	4.65	1.55
V_4C_3	3.86	1.29	V_4N_3	3.04	1.01
W_4C_3	1.86	0.62	W_4N_3	0.78	0.26
Zr_4C_3	7.35	2.45	Zr_4N_3	4.60	1.53

Table S4. Standard electrode potentials of half reactions relevant to the studied SAC-like sites of MXenes. The standard potentials (E^{o}) are provided in volts (V) relative to the standard hydrogen electrode (SHE).

Element	Half Reaction	$E°$ / V	Electrons Transferred
Cr	$Cr^{2+} + 2e^- \rightleftharpoons Cr_{(s)}$	-0.91	2
	$Cr^{3+} + 3e^- \rightleftharpoons Cr_{(s)}$	-0.74	3
Fe	$Fe^{2+} + 2e^- \rightleftharpoons Fe_{(s)}$	-0.44	2
	$Fe^{3+} + 3e^- \rightleftharpoons Fe_{(s)}$	-0.04	3
	$FeO_4^{2-} + 6e^- + 8H^+ \rightleftharpoons Fe_{(s)} + 4H_2O$	1.08	6
Hf	$HfO(OH)_2 + 4H^+ + 4e^- \rightleftharpoons Hf_{(s)} + 3H_2O$	-1.67	4
	$HfO^{2+} + 4H^+ + 4e^- \rightleftharpoons Hf_{(s)} + H_2O$	-1.72	4
Mo	$Mo^{3+} + 3e^- \rightleftharpoons Mo_{(s)}$	-0.21	3
Nb	$Nb^{3+} + 3e^- \rightleftharpoons Nb_{(s)}$	-1.10	3
Ta	$Ta^{3+} + 3e^- \rightleftharpoons Ta_{(s)}$	-0.60	3
Ti	$TiO^{2+} + 4e^- + 2H^+ \rightleftharpoons Ti_{(s)} + H_2O$	-0.93	4
	$Ti^{3+} + 3e^- \rightleftharpoons Ti_{(s)}$	-1.37	3
	$Ti^{2+} + 2e^- \rightleftharpoons Ti_{(s)}$	-1.63	2
V	$V^{2+} + 2e^- \rightleftharpoons V_{(s)}$	-1.13	2
	$V^{3+} + 3e^- \rightleftharpoons V_{(s)}$	-0.84	3

	$VOH^{2+} + 3e^- + H^+ \rightleftharpoons V_{(s)} + H_2O$	-0.78	3
	$VO^{2+} + 4e^- + 2H^+ \rightleftharpoons V_{(s)} + H_2O$	-0.55	4
	$VO_2^+ + 5e^- + 4H^+ \rightleftharpoons V_{(s)} + H_2O$	-0.24	5
	$VO(OH)^+ + 4e^- + 3H^+ \rightleftharpoons V_{(s)} + 2H_2O$	-0.47	4
W	$WO_{3(aq)} + 6e^- + 6H^+ \rightleftharpoons W_{(s)} + 3H_2O$	-0.09	6
Zr	$Zr^{4+} + 4e^- \rightleftharpoons Zr_{(s)}$	-1.45	4

Table S5. Summary of the thermodynamic stability of screened nitrogen doped SAC-like sites on the MXene basal plane, 3N*-M_{SAC}-*O, of M_2C_1O MXene (M = Cr, Fe, Mo, Ta, and W) in the context of the *a)* pre-OER scenario (*cf.* **Figure S1**) using gas-phase DFT calculations. M^{n+} represents different ions resulting from the dissolution of the corresponding metal atom at the SAC site into solution, n is total number of electron transfers in the overall reaction, ΔG is the Gibbs free energy of the dissolution process, and U_{diss} denotes the dissolution potential relative to the SHE.

M_2C_1O	M^{n+}	n	ΔG / eV	U_{diss} / V
Cr_2C	Cr^{2+}	0	0.57	—
	Cr^{3+}	1	0.17	0.17
Fe_2C	Fe^{2+}	0	-2.20	—
	Fe^{3+}	1	-1.44	-1.44
	FeO_4^{2-}	4	5.16	1.29
Mo_2C	Mo^{3+}	1	4.65	4.65
Ta_2C	Ta^{3+}	1	4.74	4.74
W_2C	$WO_{3(aq)}$	4	3.93	0.98

Table S6. Summary of the thermodynamic stability of screened undoped SAC-like sites on the MXene basal plane, 3O*-M_{SAC}-*O, of M_2C_1O MXene (M = Cr, Fe, Mo, Ta, and W) in the context of the *a)* pre-OER scenario (*cf.* **Figure S1**) using gas-phase DFT calculations. M^{n+} represents different ions resulting from the dissolution of the corresponding metal atom at the SAC site into solution, n is total number of electron transfers in the overall reaction, ΔG is the Gibbs free energy of the dissolution process, and U_{diss} denotes the dissolution potential relative to the SHE.

M_2C_1O	M^{n+}	n	ΔG / eV	U_{diss} / V
Cr_2C	Cr^{2+}	0	0.88	—
	Cr^{3+}	1	0.48	0.48
Fe_2C	Fe^{2+}	0	1.43	—
	Fe^{3+}	1	2.19	2.19
	FeO_4^{2-}	4	8.79	2.20
Mo_2C	Mo^{3+}	1	3.25	3.25
Ta_2C	Ta^{3+}	1	2.32	2.32
W_2C	$WO_{3(aq)}$	4	-1.38	-0.35

Table S7. Summary of the thermodynamic stability of screened nitrogen doped SAC-like sites on the MXene basal plane, 3N*-M_{SAC}-*O, of M_2C_1O MXene (M = Cr, Fe, Mo, Ta, and W) in the context of the *b)* OER scenario (*cf.* **Figure S2**) using gas-phase DFT calculations. M^{n+} represents different ions resulting from the dissolution of the corresponding metal atom at the SAC site into solution, n is total number of electron transfers in the overall reaction, ΔG is the Gibbs free energy of the dissolution process, and U_{diss} denotes the dissolution potential relative to the SHE.

M_2CO	**M^{n+}**	***n***	**ΔG / eV**	**U_{diss} / V**
Cr_2C	Cr^{2+}	4	5.48	1.37
	Cr^{3+}	5	5.08	1.02
Fe_2C	Fe^{2+}	4	2.72	0.68
	Fe^{3+}	5	3.48	0.70
	FeO_4^{2-}	8	10.08	1.26
Mo_2C	Mo^{3+}	5	9.56	1.91
Ta_2C	Ta^{3+}	5	9.66	1.93
W_2C	$WO_{3(aq)}$	8	8.85	1.11

Table S8. Summary of the thermodynamic stability of screened undoped SAC-like sites on the MXene basal plane, 3O*-M_{SAC}-*O, of M_2C_1O MXene (M = Cr, Fe, Mo, Ta, and W) in the context of the *b)* OER scenario (*cf.* **Figure S2**) using gas-phase DFT calculations. M^{n+} represents different ions resulting from the dissolution of the corresponding metal atom at the SAC site into solution, n is total number of electron transfers in the overall reaction, ΔG is the Gibbs free energy of the dissolution process, and U_{diss} denotes the dissolution potential relative to the SHE.

M_2C_1O	M^{n+}	n	ΔG / eV	U_{diss} / V
Cr_2C	Cr^{2+}	4	5.80	1.45
	Cr^{3+}	5	5.40	1.08
Fe_2C	Fe^{2+}	4	6.35	1.59
	Fe^{3+}	5	7.11	1.42
	FeO_4^{2-}	8	13.71	1.71
Mo_2C	Mo^{3+}	5	8.17	1.63
Ta_2C	Ta^{3+}	5	7.24	1.45
W_2C	$WO_{3(aq)}$	8	3.53	0.44

Table S9. Summary of the thermodynamic stability of screened nitrogen doped SAC-like sites on the MXene basal plane, 3N*-M_{SAC}-*O, of M_2N_1O MXene (M = Cr, Mo, Ta, V and W) in the context of the *a)* pre-OER scenario (*cf.* **Figure S1**) using gas-phase DFT calculations. M^{n+} represents different ions resulting from the dissolution of the corresponding metal atom at the SAC site into solution, n is total number of electron transfers in the overall reaction, ΔG is the Gibbs free energy of the dissolution process, and U_{diss} denotes the dissolution potential relative to the SHE.

M_2N_1O	M^{n+}	n	ΔG / eV	U_{diss} / V
Cr_2N	Cr^{2+}	0	0.12	—
	Cr^{3+}	1	-0.28	-0.28
Mo_2N	Mo^{3+}	1	4.46	4.46
Ta_2N	Ta^{3+}	1	3.95	3.95
V_2N	V^{2+}	0	1.63	—
	V^{3+}	1	1.37	1.37
	VOH^{2+}	1	1.55	1.55
	VO^{2+}	2	1.69	0.84
	VO_2^{+}	3	2.69	0.90
	$VO(OH)^{+}$	2	2.01	1.00
W_2N	$WO_{3(aq)}$	4	2.95	0.74

Table S10. Summary of the thermodynamic stability of screened undoped SAC-like sites on the MXene basal plane, 3O*-M_{SAC}-*O, of M_2N_1O MXene (M = Cr, Mo, Ta, V and W) in the context of the *a)* pre-OER scenario (*cf.* **Figure S1**) using gas-phase DFT calculations. M^{n+} represents different ions resulting from the dissolution of the corresponding metal atom at the SAC site into solution, *n* is total number of electron transfers in the overall reaction, ΔG is the Gibbs free energy of the dissolution process, and U_{diss} denotes the dissolution potential relative to the SHE.

M_2N_1O	M^{n+}	*n*	ΔG / eV	U_{diss} / V
Cr_2N	Cr^{2+}	0	1.07	—
	Cr^{3+}	1	0.67	0.67
Mo_2N	Mo^{3+}	1	1.63	1.63
Ta_2N	Ta^{3+}	1	2.31	2.31
V_2N	V^{2+}	0	1.04	—
	V^{3+}	1	0.78	0.78
	VOH^{2+}	1	0.96	0.96
	VO^{2+}	2	1.10	0.55
	VO_2^{+}	3	2.10	0.70
	$VO(OH)^{+}$	2	1.42	0.71
W_2N	$WO_{3(aq)}$	4	-0.82	-0.20

Table S11. Summary of the thermodynamic stability of screened nitrogen doped SAC-like sites on the MXene basal plane, 3N*-M_{SAC}-*O, of M_2N_1O MXene (M = Cr, Mo, Ta, V and W) in the context of the *b)* OER scenario (*cf.* **Figure S2**) using gas-phase DFT calculations. M^{n+} represents different ions resulting from the dissolution of the corresponding metal atom at the SAC site into solution, *n* is total number of electron transfers in the overall reaction, ΔG is the Gibbs free energy of the dissolution process, and U_{diss} denotes the dissolution potential relative to the SHE.

M_2N_1O	M^{n+}	*n*	ΔG / eV	U_{diss} / V
Cr_2N	Cr^{2+}	4	5.04	1.26
	Cr^{3+}	5	4.64	0.93
Mo_2N	Mo^{3+}	5	9.37	1.87
Ta_2N	Ta^{3+}	5	8.87	1.77
V_2N	V^{2+}	4	6.54	1.64
	V^{3+}	5	6.28	1.26
	VOH^{2+}	5	6.46	1.29
	VO^{2+}	6	6.60	1.10
	VO_2^{+}	7	7.60	1.09
	$VO(OH)^{+}$	6	6.92	1.15
W_2N	$WO_{3(aq)}$	8	7.87	0.98

Table S12. Summary of the thermodynamic stability of screened undoped SAC-like sites on the MXene basal plane, 3O*-M_{SAC}-*O, of M_2N_1O MXene (M = Cr, Mo, Ta, V and W) in the context of the *b)* OER scenario (*cf.* **Figure S2**) using gas-phase DFT calculations. M^{n+} represents different ions resulting from the dissolution of the corresponding metal atom at the SAC site into solution, n is total number of electron transfers in the overall reaction, ΔG is the Gibbs free energy of the dissolution process, and U_{diss} denotes the dissolution potential relative to the SHE.

M_2N_1O	M^{n+}	n	ΔG / eV	U_{diss} / V
Cr_2N	Cr^{2+}	4	5.99	1.45
	Cr^{3+}	5	5.59	1.12
Mo_2N	Mo^{3+}	5	6.55	1.31
Ta_2N	Ta^{3+}	5	7.23	1.45
V_2N	V^{2+}	4	5.96	1.49
	V^{3+}	5	5.70	1.14
	VOH^{2+}	5	5.88	1.18
	VO^{2+}	6	6.02	1.00
	VO_2^{+}	7	7.02	1.00
	$VO(OH)^{+}$	6	6.34	1.06
W_2N	$WO_{3(aq)}$	8	4.10	0.51

Table S13. Summary of the thermodynamic stability of screened nitrogen doped SAC-like sites on the MXene basal plane, 3N*-M_{SAC}-*O, of M_3C_2O MXene (M = Mo, Nb, Ta, V and W) in the context of the *a)* pre-OER scenario (*cf.* **Figure S1**) using gas-phase DFT calculations. M^{n+} represents different ions resulting from the dissolution of the corresponding metal atom at the SAC site into solution, n is total number of electron transfers in the overall reaction, ΔG is the Gibbs free energy of the dissolution process, and U_{diss} denotes the dissolution potential relative to the SHE.

M_3C_2O	M^{n+}	n	ΔG / eV	U_{diss} / V
Mo_3C_2	Mo^{3+}	1	4.55	4.55
Nb_3C_2	Nb^{3+}	1	0.69	0.69
Ta_3C_2	Ta^{3+}	1	2.38	2.38
V_3C_2	V^{2+}	0	1.61	—
	V^{3+}	1	1.35	1.35
	VOH^{2+}	1	1.53	1.53
	VO^{2+}	2	1.67	0.84
	VO_2^{+}	3	2.67	0.89
	$VO(OH)^{+}$	2	1.99	1.00
W_3C_2	$WO_{3(aq)}$	4	4.32	1.08

Table S14. Summary of the thermodynamic stability of screened undoped SAC-like sites on the MXene basal plane, 3O*-M_{SAC}-*O, of M_3C_2O MXene (M = Mo, Nb, Ta, V and W) in the context of the *a)* pre-OER scenario (*cf.* **Figure S1**) using gas-phase DFT calculations. M^{n+} represents different ions resulting from the dissolution of the corresponding metal atom at the SAC site into solution, *n* is total number of electron transfers in the overall reaction, ΔG is the Gibbs free energy of the dissolution process, and U_{diss} denotes the dissolution potential relative to the SHE.

M_3C_2O	M^{n+}	*n*	ΔG / eV	U_{diss} / V
Mo_3C_2	Mo^{3+}	1	3.00	3.00
Nb_3C_2	Nb^{3+}	1	-0.90	-0.90
Ta_3C_2	Ta^{3+}	1	0.14	0.14
V_3C_2	V^{2+}	0	1.11	—
	V^{3+}	1	0.85	0.85
	VOH^{2+}	1	1.03	1.03
	VO^{2+}	2	1.17	0.58
	VO_2^{+}	3	2.17	0.72
	$VO(OH)^{+}$	2	1.49	0.74
W_3C_2	$WO_{3(aq)}$	4	1.11	0.28

Table S15. Summary of the thermodynamic stability of screened nitrogen doped SAC-like sites on the MXene basal plane, 3N*-M_{SAC}-*O, of M_3C_2O MXene (M = Mo, Nb, Ta, V and W) in the context of the *b)* OER scenario (*cf.* **Figure S2**) using gas-phase DFT calculations. M^{n+} represents different ions resulting from the dissolution of the corresponding metal atom at the SAC site into solution, *n* is total number of electron transfers in the overall reaction, ΔG is the Gibbs free energy of the dissolution process, and U_{diss} denotes the dissolution potential relative to the SHE.

M_3C_2O	M^{n+}	*n*	ΔG / eV	U_{diss} / V
Mo_3C_2	Mo^{3+}	5	9.47	1.89
Nb_3C_2	Nb^{3+}	5	5.61	1.12
Ta_3C_2	Ta^{3+}	5	7.30	1.46
V_3C_2	V^{2+}	4	6.53	1.63
	V^{3+}	5	6.27	1.25
	VOH^{2+}	5	6.45	1.29
	VO^{2+}	6	6.59	1.10
	VO_2^{+}	7	7.59	1.08
	$VO(OH)^{+}$	6	6.91	1.15
W_3C_2	$WO_{3(aq)}$	8	9.23	1.15

Table S16. Summary of the thermodynamic stability of screened undoped SAC-like sites on the MXene basal plane, 3O*-M_{SAC}-*O, of M_3C_2O MXene (M = Mo, Nb, Ta, V and W) in the context of the *b)* OER scenario (*cf.* **Figure S2**) using gas-phase DFT calculations. M^{n+} represents different ions resulting from the dissolution of the corresponding metal atom at the SAC site into solution, *n* is total number of electron transfers in the overall reaction, ΔG is the Gibbs free energy of the dissolution process, and U_{diss} denotes the dissolution potential relative to the SHE.

M_3C_2O	M^{n+}	*n*	ΔG / eV	U_{diss} / V
Mo_3C_2	Mo^{3+}	5	7.92	1.58
Nb_3C_2	Nb^{3+}	5	4.02	0.80
Ta_3C_2	Ta^{3+}	5	5.06	1.01
V_3C_2	V^{2+}	4	6.03	1.51
	V^{3+}	5	5.77	1.15
	VOH^{2+}	5	5.95	1.19
	VO^{2+}	6	6.09	1.01
	VO_2^{+}	7	7.09	1.01
	$VO(OH)^{+}$	6	6.41	1.07
W_3C_2	$WO_{3(aq)}$	8	6.03	0.75

Table S17. Summary of the thermodynamic stability of screened undoped SAC-like sites on the MXene basal plane, 3N*-M_{SAC}-*O, of M_3N_2O MXene (M = Cr, Hf, Mo, Nb, V, W, and Zr) in the context of the *a)* pre-OER scenario (*cf.* **Figure S1**) using gas-phase DFT calculations. M^{n+} represents different ions resulting from the dissolution of the corresponding metal atom at the SAC site into solution, n is total number of electron transfers in the overall reaction, ΔG is the Gibbs free energy of the dissolution process, and U_{diss} denotes the dissolution potential relative to the SHE.

M_3N_2O	M^{n+}	n	ΔG / eV	U_{diss} / V
Cr_3N_2	Cr^{2+}	0	1.17	—
	Cr^{3+}	1	0.77	0.77
Hf_3N_2	$HfO(OH)_2$	2	-0.72	-0.36
	HfO^{2+}	2	-0.94	-0.47
Mo_3N_2	Mo^{3+}	1	4.78	4.78
Nb_3N_2	Nb^{3+}	1	0.27	0.27
V_3N_2	V^{2+}	0	1.09	—
	V^{3+}	1	0.83	0.83
	VOH^{2+}	1	1.01	1.01
	VO^{2+}	2	1.15	0.58
	VO_2^{+}	3	2.15	0.72
	$VO(OH)^{+}$	2	1.47	0.74
W_3N_2	$WO_{3(aq)}$	4	3.38	0.85
Zr_3N_2	Zr^{4+}	2	-0.09	-0.04

Table S18. Summary of the thermodynamic stability of screened undoped SAC-like sites on the MXene basal plane, 3O*-M_{SAC}-*O, of M_3N_2O MXene (M = Cr, Hf, Mo, Nb, V, W, and Zr) in the context of the *a)* pre-OER scenario (*cf.* **Figure S1**) using gas-phase DFT calculations. M^{n+} represents different ions resulting from the dissolution of the corresponding metal atom at the SAC site into solution, n is total number of electron transfers in the overall reaction, ΔG is the Gibbs free energy of the dissolution process, and U_{diss} denotes the dissolution potential relative to the SHE.

M_3N_2O	M^{n+}	n	ΔG / eV	U_{diss} / V
Cr_3N_2	Cr^{2+}	0	1.14	—
	Cr^{3+}	1	0.74	0.74
Hf_3N_2	$HfO(OH)_2$	2	-4.46	-2.23
	HfO^{2+}	2	-4.68	-2.34
Mo_3N_2	Mo^{3+}	1	1.93	1.93
Nb_3N_2	Nb^{3+}	1	-0.86	-0.86
V_3N_2	V^{2+}	0	0.26	—
	V^{3+}	1	0.00	0.00
	VOH^{2+}	1	0.18	0.18
	VO^{2+}	2	0.32	0.16
	VO_2^{+}	3	1.32	0.44
	$VO(OH)^{+}$	2	0.64	0.32
W_3N_2	$WO_{3(aq)}$	4	-0.36	-0.09
Zr_3N_2	Zr^{4+}	2	-2.96	-1.48

Table S19. Summary of the thermodynamic stability of screened nitrogen doped SAC-like sites on the MXene basal plane, 3N*-M_{SAC}-*O, of M_3N_2O MXene (M = Cr, Hf, Mo, Nb, V, W, and Zr) in the context of the *b)* OER scenario (*cf.* **Figure S2**) using gas-phase DFT calculations. M^{n+} represents different ions resulting from the dissolution of the corresponding metal atom at the SAC site into solution, n is total number of electron transfers in the overall reaction, ΔG is the Gibbs free energy of the dissolution process, and U_{diss} denotes the dissolution potential relative to the SHE.

M_3N_2O	M^{n+}	n	ΔG / eV	U_{diss} / V
Cr_3N_2	Cr^{2+}	4	6.09	1.52
	Cr^{3+}	5	5.69	1.14
Hf_3N_2	$HfO(OH)_2$	6	4.20	0.70
	HfO^{2+}	6	3.98	0.66
Mo_3N_2	Mo^{3+}	5	9.69	1.94
Nb_3N_2	Nb^{3+}	5	5.19	1.04
V_3N_2	V^{2+}	4	6.01	1.50
	V^{3+}	5	5.75	1.15
	VOH^{2+}	5	5.93	1.19
	VO^{2+}	6	6.07	1.01
	VO_2^{+}	7	7.07	1.01
	$VO(OH)^{+}$	6	6.39	1.07
W_3N_2	$WO_{3(aq)}$	8	8.30	1.04
Zr_3N_2	Zr^{4+}	6	4.83	0.81

Table S20. Summary of the thermodynamic stability of screened nitrogen doped SAC-like sites on the MXene basal plane, 3O*-M_{SAC}-*O, of M_3N_2O MXene (M = Cr, Hf, Mo, Nb, V, W, and Zr) in the context of the *b)* OER scenario (*cf.* **Figure S2**) using gas-phase DFT calculations. M^{n+} represents different ions resulting from the dissolution of the corresponding metal atom at the SAC site into solution, n is total number of electron transfers in the overall reaction, ΔG is the Gibbs free energy of the dissolution process, and U_{diss} denotes the dissolution potential relative to the SHE.

M_3N_2O	M^{n+}	n	ΔG / eV	U_{diss} / V
Cr_3N_2	Cr^{2+}	4	6.05	1.51
	Cr^{3+}	5	5.65	1.13
Hf_3N_2	$HfO(OH)_2$	6	0.46	0.08
	HfO^{2+}	6	0.24	0.04
Mo_3N_2	Mo^{3+}	5	6.85	1.37
Nb_3N_2	Nb^{3+}	5	4.05	0.81
V_3N_2	V^{2+}	4	5.18	1.29
	V^{3+}	5	4.92	0.98
	VOH^{2+}	5	5.10	1.02
	VO^{2+}	6	5.24	0.87
	VO_2^{+}	7	6.24	0.89
	$VO(OH)^{+}$	6	5.56	0.93
W_3N_2	$WO_{3(aq)}$	8	4.56	0.57
Zr_3N_2	Zr^{4+}	6	1.95	0.33

Table S21. Summary of the thermodynamic stability of screened nitrogen doped SAC-like sites on the MXene basal plane, 3N*-M_{SAC}-*O, of M_4C_3O MXene (M = Mo, Nb, Ta and W) in the context of the *a)* pre-OER scenario (*cf.* **Figure S1**) using gas-phase DFT calculations. M^{n+} represents different ions resulting from the dissolution of the corresponding metal atom at the SAC site into solution, n is total number of electron transfers in the overall reaction, ΔG is the Gibbs free energy of the dissolution process, and U_{diss} denotes the dissolution potential relative to the SHE.

M_4C_3O	M^{n+}	n	ΔG / eV	U_{diss} / V
Mo_4C_3	Mo^{3+}	1	4.49	4.49
Nb_4C_3	Nb^{3+}	1	1.21	1.21
Ta_4C_3	Ta^{3+}	1	3.24	3.24
W_4C_3	$WO_{3(aq)}$	4	4.37	1.09

Table S22. Summary of the thermodynamic stability of screened undoped SAC-like sites on the MXene basal plane, 3O*-M_{SAC}-*O, of M_4C_3O MXene (M = Mo, Nb, Ta and W) in the context of the *a)* pre-OER scenario (*cf.* **Figure S1**) using gas-phase DFT calculations. M^{n+} represents different ions resulting from the dissolution of the corresponding metal atom at the SAC site into solution, *n* is total number of electron transfers in the overall reaction, ΔG is the Gibbs free energy of the dissolution process, and U_{diss} denotes the dissolution potential relative to the SHE.

M_4C_3O	M^{n+}	*n*	ΔG / eV	U_{diss} / V
Mo_4C_3	Mo^{3+}	1	3.04	3.04
Nb_4C_3	Nb^{3+}	1	0.07	0.07
Ta_4C_3	Ta^{3+}	1	1.21	1.21
W_4C_3	$WO_{3(aq)}$	4	1.26	0.31

Table S23. Summary of the thermodynamic stability of screened nitrogen doped SAC-like sites on the MXene basal plane, 3N*-M_{SAC}-*O, of M_4C_3O MXene (M = Mo, Nb, Ta and W) in the context of the *b)* OER scenario (*cf.* **Figure S2**) using gas-phase DFT calculations. M^{n+} represents different ions resulting from the dissolution of the corresponding metal atom at the SAC site into solution, *n* is total number of electron transfers in the overall reaction, ΔG is the Gibbs free energy of the dissolution process, and U_{diss} denotes the dissolution potential relative to the SHE.

M_4C_3O	M^{n+}	*n*	ΔG / eV	U_{diss} / V
Mo_4C_3	Mo^{3+}	5	9.41	1.88
Nb_4C_3	Nb^{3+}	5	6.13	1.23
Ta_4C_3	Ta^{3+}	5	8.15	1.63
W_4C_3	$WO_{3(aq)}$	8	9.29	1.16

Table S24. Summary of the thermodynamic stability of screened undoped SAC-like sites on the MXene basal plane, 3O*-M_{SAC}-*O, of M_4C_3O MXene (M = Mo, Nb, Ta and W) in the context of the *b)* OER scenario (*cf.* **Figure S2**) using gas-phase DFT calculations. M^{n+} represents different ions resulting from the dissolution of the corresponding metal atom at the SAC site into solution, n is total number of electron transfers in the overall reaction, ΔG is the Gibbs free energy of the dissolution process, and U_{diss} denotes the dissolution potential relative to the SHE.

M_4C_3O	M^{n+}	n	ΔG / eV	U_{diss} / V
Mo_4C_3	Mo^{3+}	5	7.96	1.59
Nb_4C_3	Nb^{3+}	5	4.99	1.00
Ta_4C_3	Ta^{3+}	5	6.13	1.23
W_4C_3	$WO_{3(aq)}$	8	6.18	0.77

Table S25. Summary of the thermodynamic stability of screened nitrogen doped SAC-like sites on the MXene basal plane, 3N*-M_{SAC}-*O, of M_4N_3O MXene (M = Cr, Mo, Nb, Ta, V and W) in the context of the *a)* pre-OER scenario (*cf.* **Figure S1**) using gas-phase DFT calculations. M^{n+} represents different ions resulting from the dissolution of the corresponding metal atom at the SAC site into solution, n is total number of electron transfers in the overall reaction, ΔG is the Gibbs free energy of the dissolution process, and U_{diss} denotes the dissolution potential relative to the SHE.

M_4N_3O	M^{n+}	n	ΔG / eV	U_{diss} / V
Cr_4N_3	Cr^{2+}	0	1.81	—
	Cr^{3+}	1	1.41	1.41
Mo_4N_3	Mo^{3+}	1	4.97	4.97
Nb_4N_3	Nb^{3+}	1	0.14	0.14
Ta_4N_3	Ta^{3+}	1	1.85	1.85
V_4N_3	V^{2+}	0	1.18	1.18
	V^{3+}	1	0.92	0.92
	VOH^{2+}	1	1.10	1.10
	VO^{2+}	2	1.24	0.62
	VO_2^{+}	3	2.24	0.75
	$VO(OH)^{+}$	2	1.56	0.78
W_4N_3	$WO_{3(aq)}$	4	3.54	0.89

Table S26. Summary of the thermodynamic stability of screened undoped SAC-like sites on the MXene basal plane, 3O*-M_{SAC}-*O, of M_4N_3O MXene (M = Cr, Mo, Nb, Ta, V and W) in the context of the *a)* pre-OER scenario (*cf.* **Figure S1**) using gas-phase DFT calculations. M^{n+} represents different ions resulting from the dissolution of the corresponding metal atom at the SAC site into solution, *n* is total number of electron transfers in the overall reaction, ΔG is the Gibbs free energy of the dissolution process, and U_{diss} denotes the dissolution potential relative to the SHE.

M_4N_3O	M^{n+}	*n*	ΔG / eV	U_{diss} / V
Cr_4N_3	Cr^{2+}	0	1.95	—
	Cr^{3+}	1	1.55	1.55
Mo_4N_3	Mo^{3+}	1	2.04	2.04
Nb_4N_3	Nb^{3+}	1	-1.25	-1.25
Ta_4N_3	Ta^{3+}	1	0.15	0.15
V_4N_3	V^{2+}	0	0.44	—
	V^{3+}	1	0.18	0.18
	VOH^{2+}	1	0.36	0.36
	VO^{2+}	2	0.50	0.25
	VO_2^{+}	3	1.50	0.50
	$VO(OH)^{+}$	2	0.82	0.41
W_4N_3	$WO_{3(aq)}$	4	-0.39	-0.10

Table S27. Summary of the thermodynamic stability of screened nitrogen doped SAC-like sites on the MXene basal plane, 3N*-M_{SAC}-*O, of M_4N_3O MXene (M = Cr, Mo, Nb, Ta, V and W) in the context of the *b)* OER scenario (*cf.* **Figure S2**) using gas-phase DFT calculations. M^{n+} represents different ions resulting from the dissolution of the corresponding metal atom at the SAC site into solution, *n* is total number of electron transfers in the overall reaction, ΔG is the Gibbs free energy of the dissolution process, and U_{diss} denotes the dissolution potential relative to the SHE.

M_4N_3O	M^{n+}	*n*	ΔG / eV	U_{diss} / V
Cr_4N_3	Cr^{2+}	4	6.73	1.68
	Cr^{3+}	5	6.33	1.27
Mo_4N_3	Mo^{3+}	5	9.89	1.98
Nb_4N_3	Nb^{3+}	5	5.05	1.01
Ta_4N_3	Ta^{3+}	5	6.77	1.35
V_4N_3	V^{2+}	4	6.10	1.53
	V^{3+}	5	5.84	1.17
	VOH^{2+}	5	6.02	1.20
	VO^{2+}	6	6.16	1.03
	VO_2^{+}	7	7.16	1.02
	$VO(OH)^{+}$	6	6.48	1.08
W_4N_3	$WO_{3(aq)}$	8	8.46	1.06

Table S28. Summary of the thermodynamic stability of screened undoped SAC-like sites on the MXene basal plane, 3O*-M_{SAC}-*O, of M_4N_3O MXene (M = Cr, Mo, Nb, Ta, V and W) in the context of the *b)* OER scenario (*cf.* **Figure S2**) using gas-phase DFT calculations. M^{n+} represents different ions resulting from the dissolution of the corresponding metal atom at the SAC site into solution, *n* is total number of electron transfers in the overall reaction, ΔG is the Gibbs free energy of the dissolution process, and U_{diss} denotes the dissolution potential relative to the SHE.

M_4N_3O	M^{n+}	*n*	ΔG / eV	U_{diss} / V
Cr_4N_3	Cr^{2+}	4	6.87	—
	Cr^{3+}	5	6.47	1.29
Mo_4N_3	Mo^{3+}	5	6.95	1.39
Nb_4N_3	Nb^{3+}	5	3.67	0.73
Ta_4N_3	Ta^{3+}	5	5.06	1.01
V_4N_3	V^{2+}	4	5.36	1.34
	V^{3+}	5	5.10	1.02
	VOH^{2+}	5	5.28	1.06
	VO^{2+}	6	5.42	0.90
	VO_2^{+}	7	6.42	0.92
	$VO(OH)^{+}$	6	5.74	0.96
W_4N_3	$WO_{3(aq)}$	8	4.52	0.57

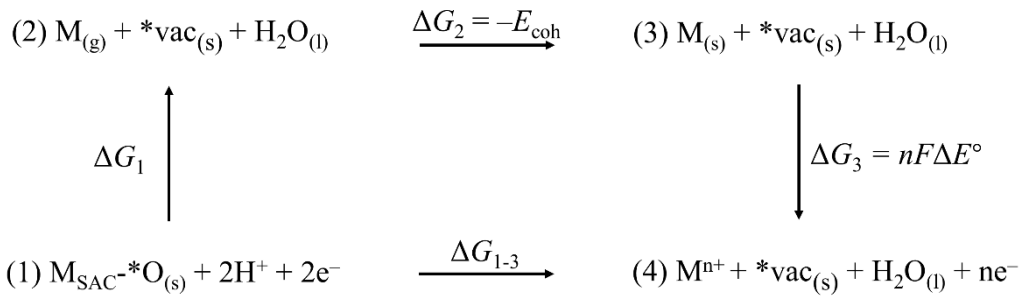

Figure S1. Thermodynamic cycle to determine the Gibbs free energy of the dissolution process of M_{SAC}-*O in the case that no oxygen is formed. Reproduced with permission from Ref. [1]

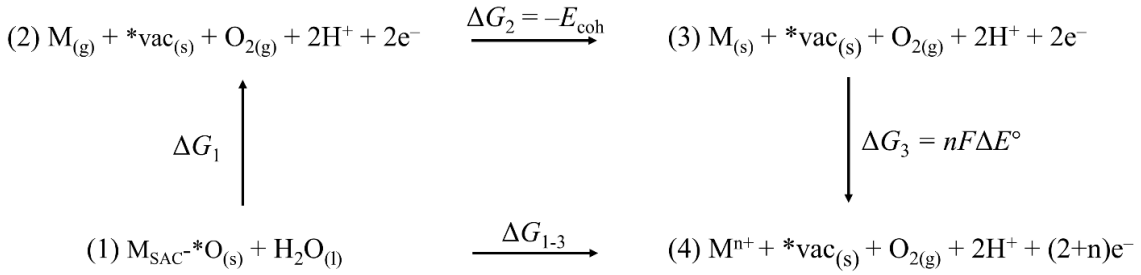

Figure S2. Thermodynamic cycle to determine the Gibbs free energy of the dissolution process of M_{SAC}-*O in the case that oxygen is formed. Reproduced with permission from Ref. [1]

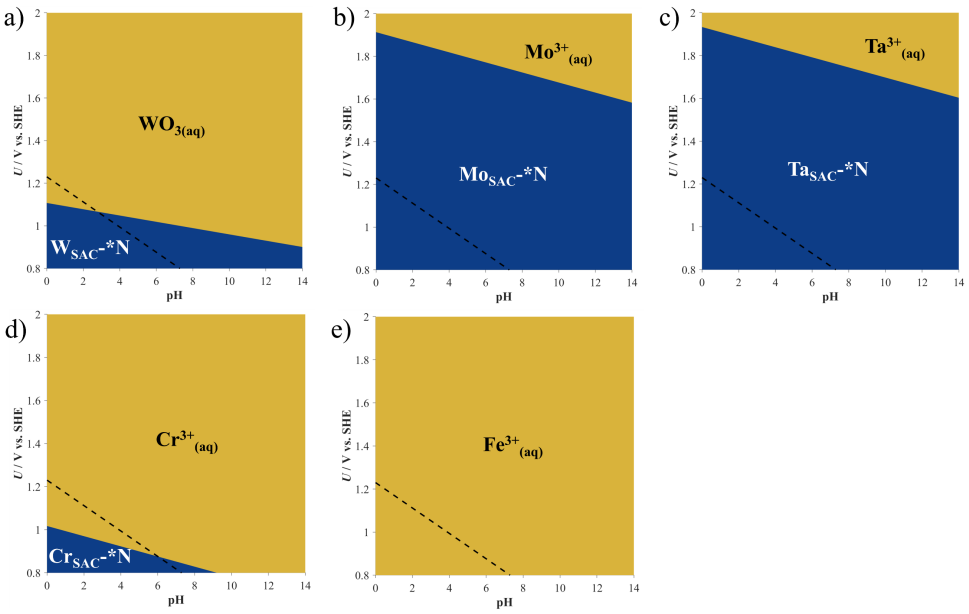

Figure S3. Pourbaix diagrams assessing the thermodynamic stability of SAC-like sites on the MXene basal plane, 3N*-M_{SAC}-*O, of a) W_2C_1O, b) Mo_2C_1O, c) Ta_2C_1O, d) Cr_2C_1O and e) Fe_2C_1O MXenes in the context of the OER scenario (*cf.* **Figure S2**). The stability of M_{SAC} is referenced to different oxidative ion states resulting from the dissolution of the corresponding metals (*cf.* **Table S4** in the SI). Regions where 3N*-M_{SAC}-*O is thermodynamically stable are colored blue, while a yellow background indicates that metal cations are energetically favored. The black, dashed line indicates the OER equilibrium potential on the SHE scale.

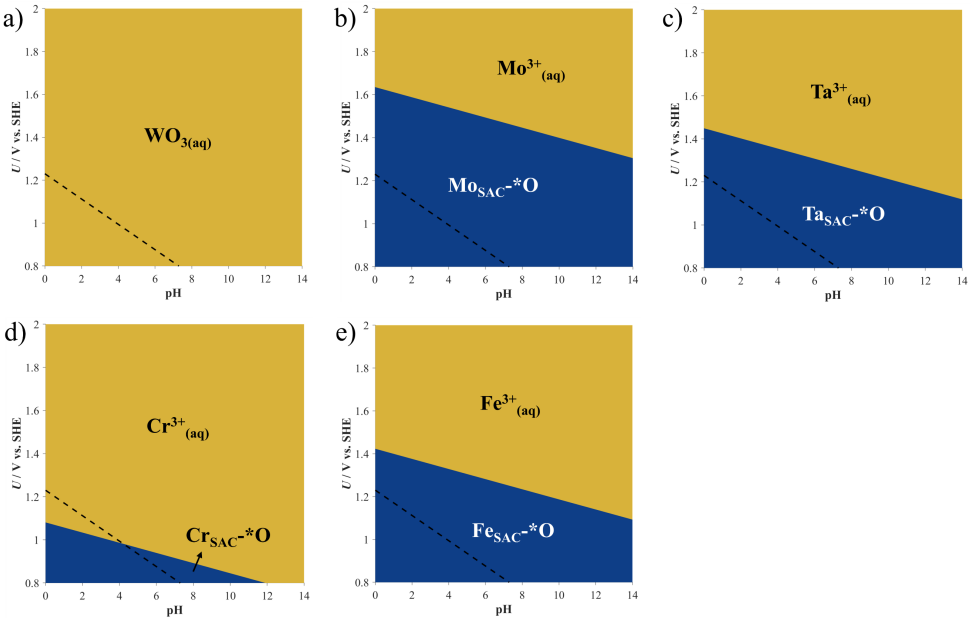

Figure S4. Pourbaix diagrams assessing the thermodynamic stability of SAC-like sites on the MXene basal plane, 3O*-M_{SAC}-*O, of a) W_2C_1O, b) Mo_2C_1O, c) Ta_2C_1O, d) Cr_2C_1O and e) Fe_2C_1O MXenes in the context of the OER scenario (*cf.* **Figure S2**). The stability of M_{SAC} is referenced to different oxidative ion states resulting from the dissolution of the corresponding metals (*cf.* **Table S4** in the SI). Regions where 3O*-M_{SAC}-*O is thermodynamically stable are colored blue, while a yellow background indicates that metal cations are energetically favored. The black, dashed line indicates the OER equilibrium potential on the SHE scale.

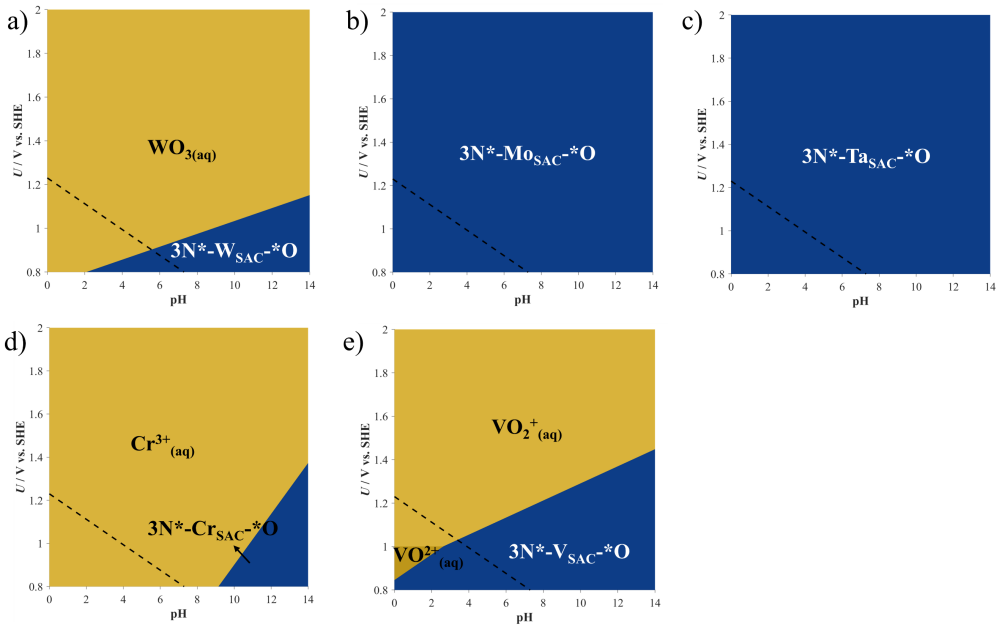

Figure S5. Pourbaix diagrams assessing the thermodynamic stability of SAC-like sites on the MXene basal plane, 3N*-M_{SAC}-*O, of a) W_2N_1O, b) Mo_2N_1O, c) Ta_2N_1O, d) Cr_2N_1O and e) V_2N_1O MXenes in the context of the pre-OER scenario (*cf.* **Figure S1**). The stability of M_{SAC} is referenced to different oxidative ion states resulting from the dissolution of the corresponding metals (*cf.* **Table S4** in the SI). Regions where 3N*-M_{SAC}-*O is thermodynamically stable are colored blue, while a yellow background indicates that metal cations are energetically favored. The black, dashed line indicates the OER equilibrium potential on the SHE scale.

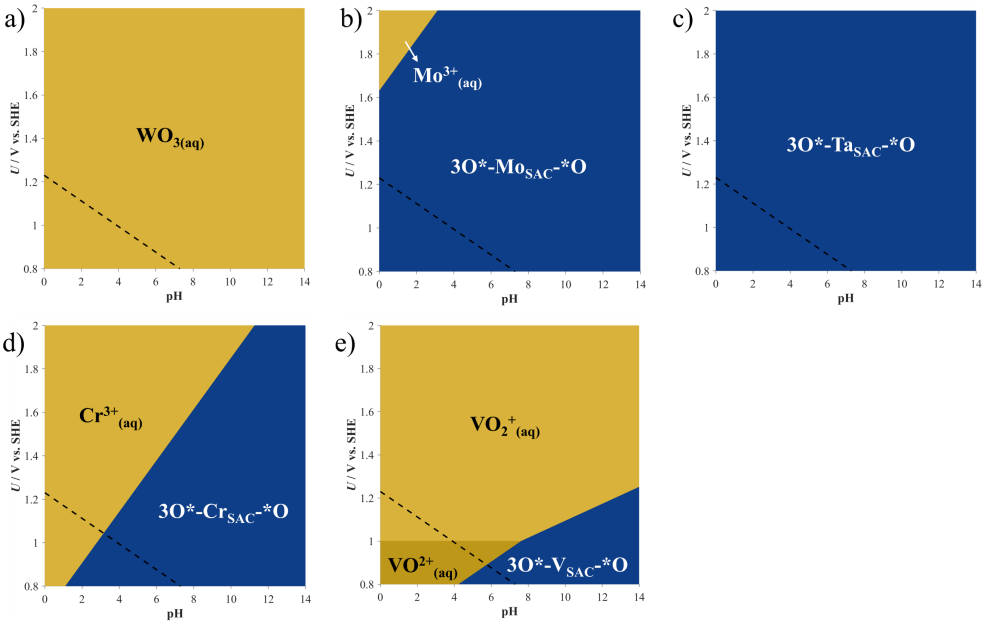

Figure S6. Pourbaix diagrams assessing the thermodynamic stability of SAC-like sites on the MXene basal plane, 3O*-M_{SAC}-*O, of a) W_2N_1O, b) Mo_2N_1O, c) Ta_2N_1O, d) Cr_2N_1O and e) V_2N_1O MXenes in the context of the pre-OER scenario (*cf.* **Figure S1**). The stability of M_{SAC} is referenced to different oxidative ion states resulting from the dissolution of the corresponding metals (*cf.* **Table S4** in the SI). Regions where 3O*-M_{SAC}-*O is thermodynamically stable are colored blue, while a yellow background indicates that metal cations are energetically favored. The black, dashed line indicates the OER equilibrium potential on the SHE scale.

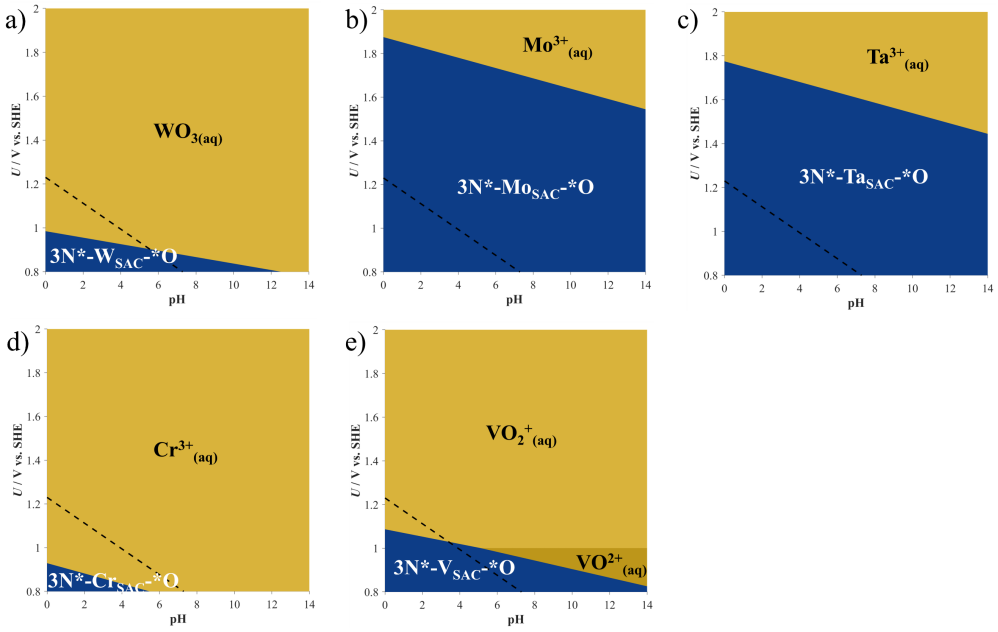

Figure S7. Pourbaix diagrams assessing the thermodynamic stability of SAC-like sites on the MXene basal plane, 3N*-M_{SAC}-*O, of a) W_2N_1O, b) Mo_2N_1O, c) Ta_2N_1O, d) Cr_2N_1O and e) V_2N_1O MXenes in the context of the OER scenario (*cf.* **Figure S2**). The stability of M_{SAC} is referenced to different oxidative ion states resulting from the dissolution of the corresponding metals (*cf.* **Table S4** in the SI). Regions where 3N*-M_{SAC}-*O is thermodynamically stable are colored blue, while a yellow background indicates that metal cations are energetically favored. The black, dashed line indicates the OER equilibrium potential on the SHE scale.

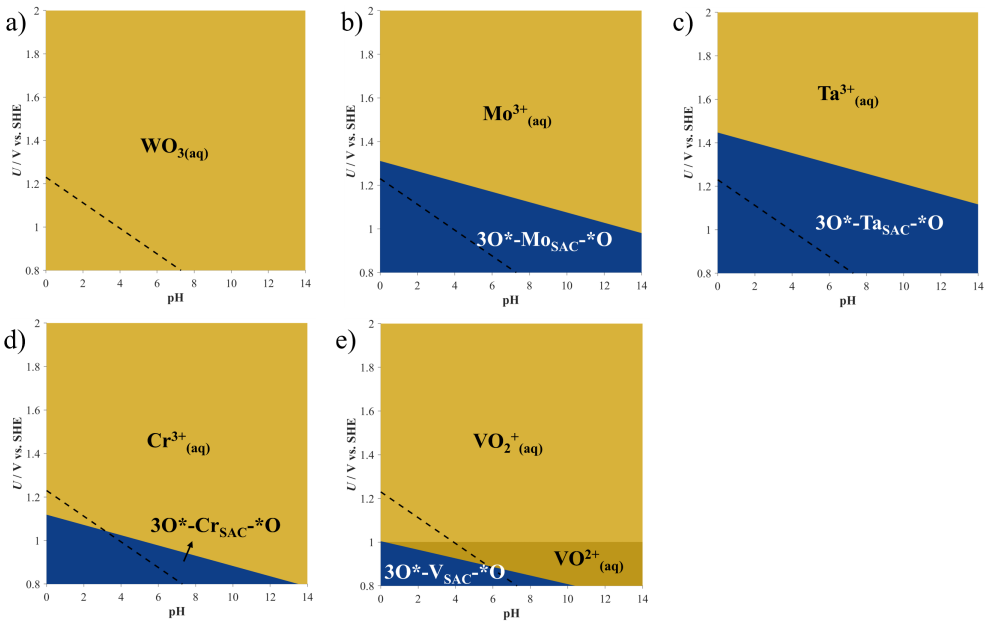

Figure S8. Pourbaix diagrams assessing the thermodynamic stability of SAC-like sites on the MXene basal plane, 3O*-M_{SAC}-*O, of a) W_2N_1O, b) Mo_2N_1O, c) Ta_2N_1O, d) Cr_2N_1O and e) V_2N_1O MXenes in the context of the OER scenario (*cf.* **Figure S2**). The stability of M_{SAC} is referenced to different oxidative ion states resulting from the dissolution of the corresponding metals (*cf.* **Table S4** in the SI). Regions where 3O*-M_{SAC}-*O is thermodynamically stable are colored blue, while a yellow background indicates that metal cations are energetically favored. The black, dashed line indicates the OER equilibrium potential on the SHE scale.

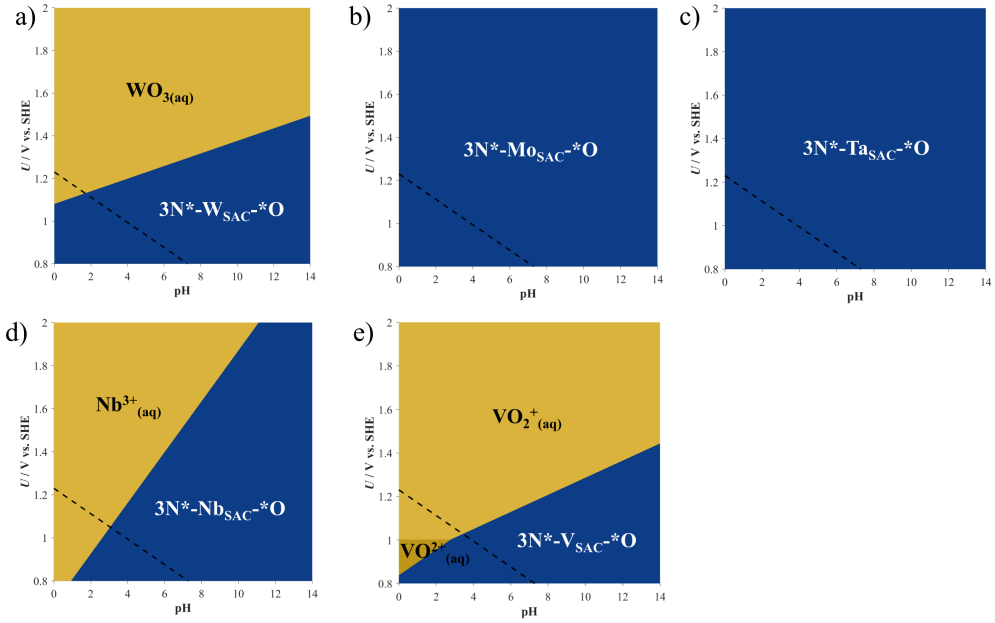

Figure S9. Pourbaix diagrams assessing the thermodynamic stability of SAC-like sites on the MXene basal plane, 3N*-M_{SAC}-*O, of a) W_3C_2O, b) Mo_3C_2O, c) Ta_3C_2O, d) Nb_3C_2O and e) V_3C_2O MXenes in the context of the pre-OER scenario (*cf.* **Figure S1**). The stability of M_{SAC} is referenced to different oxidative ion states resulting from the dissolution of the corresponding metals (*cf.* **Table S4** in the SI). Regions where 3N*-M_{SAC}-*O is thermodynamically stable are colored blue, while a yellow background indicates that metal cations are energetically favored. The black, dashed line indicates the OER equilibrium potential on the SHE scale.

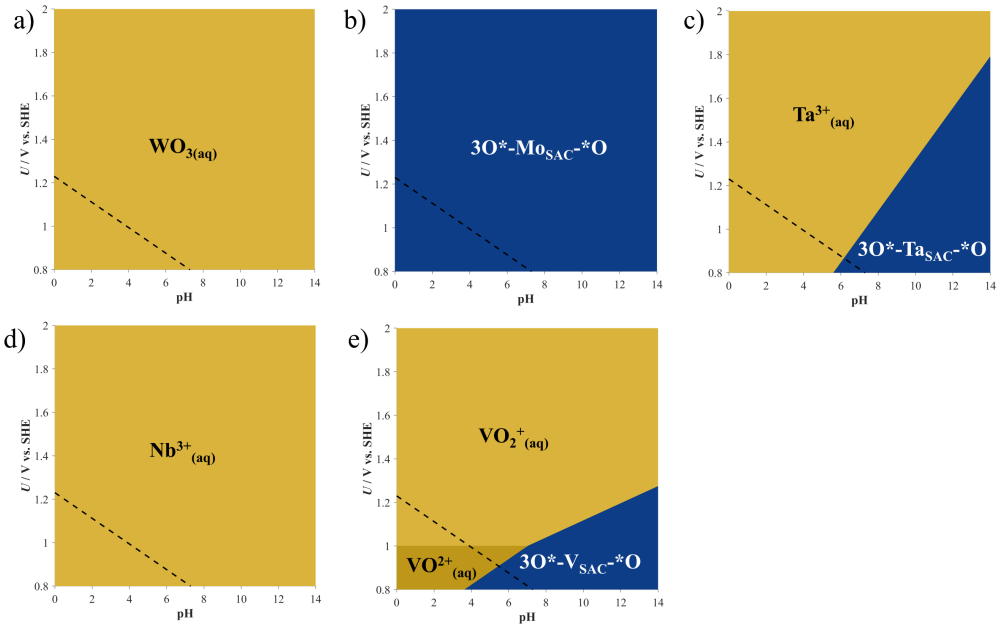

Figure S10. Pourbaix diagrams assessing the thermodynamic stability of SAC-like sites on the MXene basal plane, 3O*-M_{SAC}-*O, of a) W_3C_2O, b) Mo_3C_2O, c) Ta_3C_2O, d) Nb_3C_2O and e) V_3C_2O MXenes in the context of the pre-OER scenario (*cf.* **Figure S1**). The stability of M_{SAC} is referenced to different oxidative ion states resulting from the dissolution of the corresponding metals (*cf.* **Table S4** in the SI). Regions where 3O*-M_{SAC}-*O is thermodynamically stable are colored blue, while a yellow background indicates that metal cations are energetically favored. The black, dashed line indicates the OER equilibrium potential on the SHE scale.

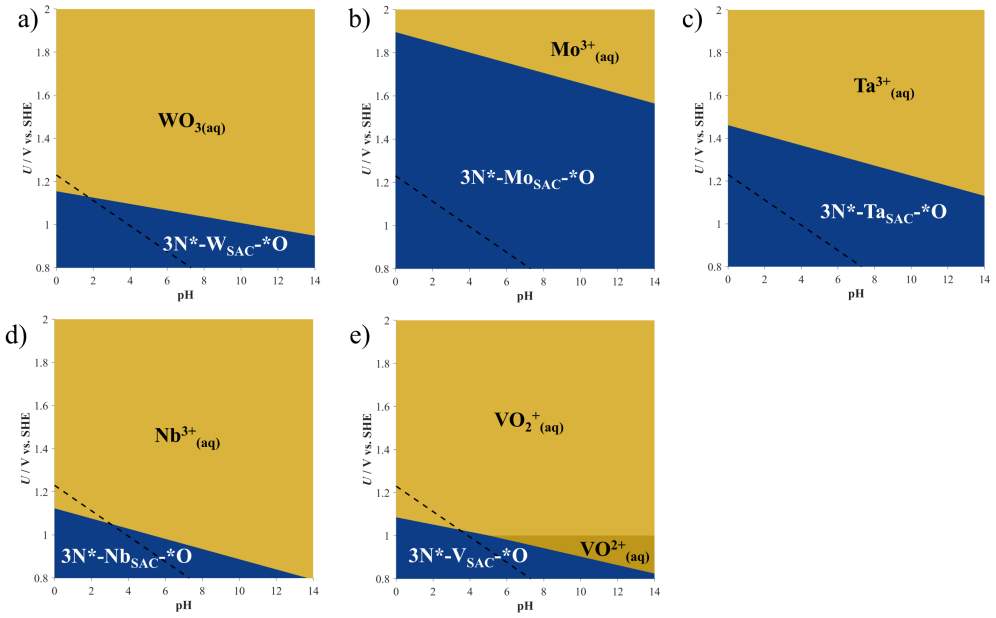

Figure S11. Pourbaix diagrams assessing the thermodynamic stability of SAC-like sites on the MXene basal plane, 3N*-M_{SAC}-*O, of a) W_3C_2O, b) Mo_3C_2O, c) Ta_3C_2O, d) Nb_3C_2O and e) V_3C_2O MXenes in the context of the OER scenario (*cf.* **Figure S2**). The stability of M_{SAC} is referenced to different oxidative ion states resulting from the dissolution of the corresponding metals (*cf.* **Table S4** in the SI). Regions where 3N*-M_{SAC}-*O is thermodynamically stable are colored blue, while a yellow background indicates that metal cations are energetically favored. The black, dashed line indicates the OER equilibrium potential on the SHE scale.

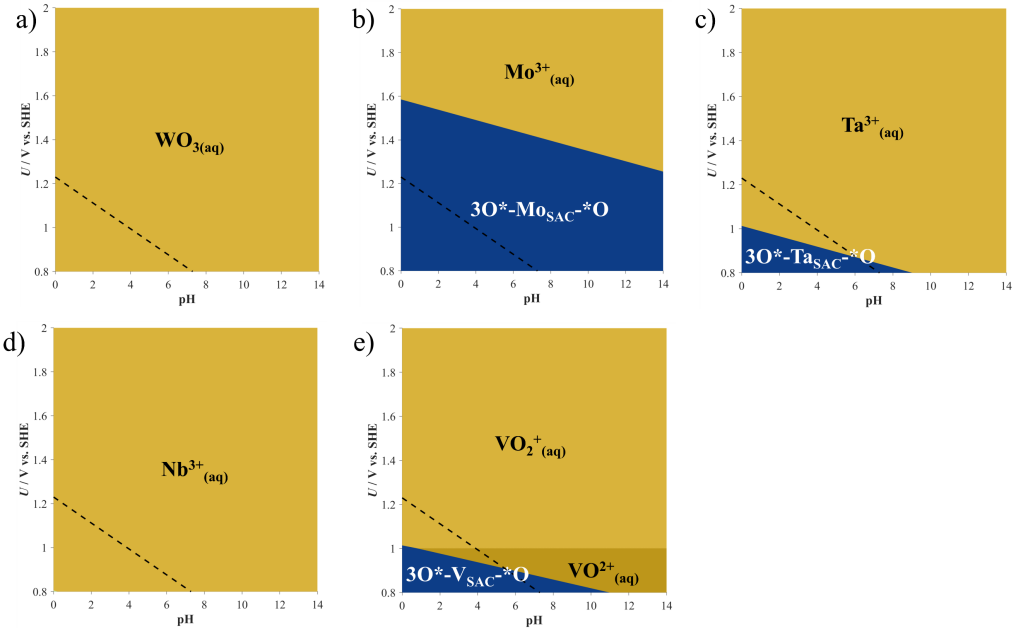

Figure S12. Pourbaix diagrams assessing the thermodynamic stability of SAC-like sites on the MXene basal plane, 3O*-M_{SAC}-*O, of a) W_3C_2O, b) Mo_3C_2O, c) Ta_3C_2O, d) Nb_3C_2O and e) V_3C_2O MXenes in the context of the OER scenario (*cf.* **Figure S2**). The stability of M_{SAC} is referenced to different oxidative ion states resulting from the dissolution of the corresponding metals (*cf.* **Table S4** in the SI). Regions where 3O*-M_{SAC}-*O is thermodynamically stable are colored blue, while a yellow background indicates that metal cations are energetically favored. The black, dashed line indicates the OER equilibrium potential on the SHE scale.

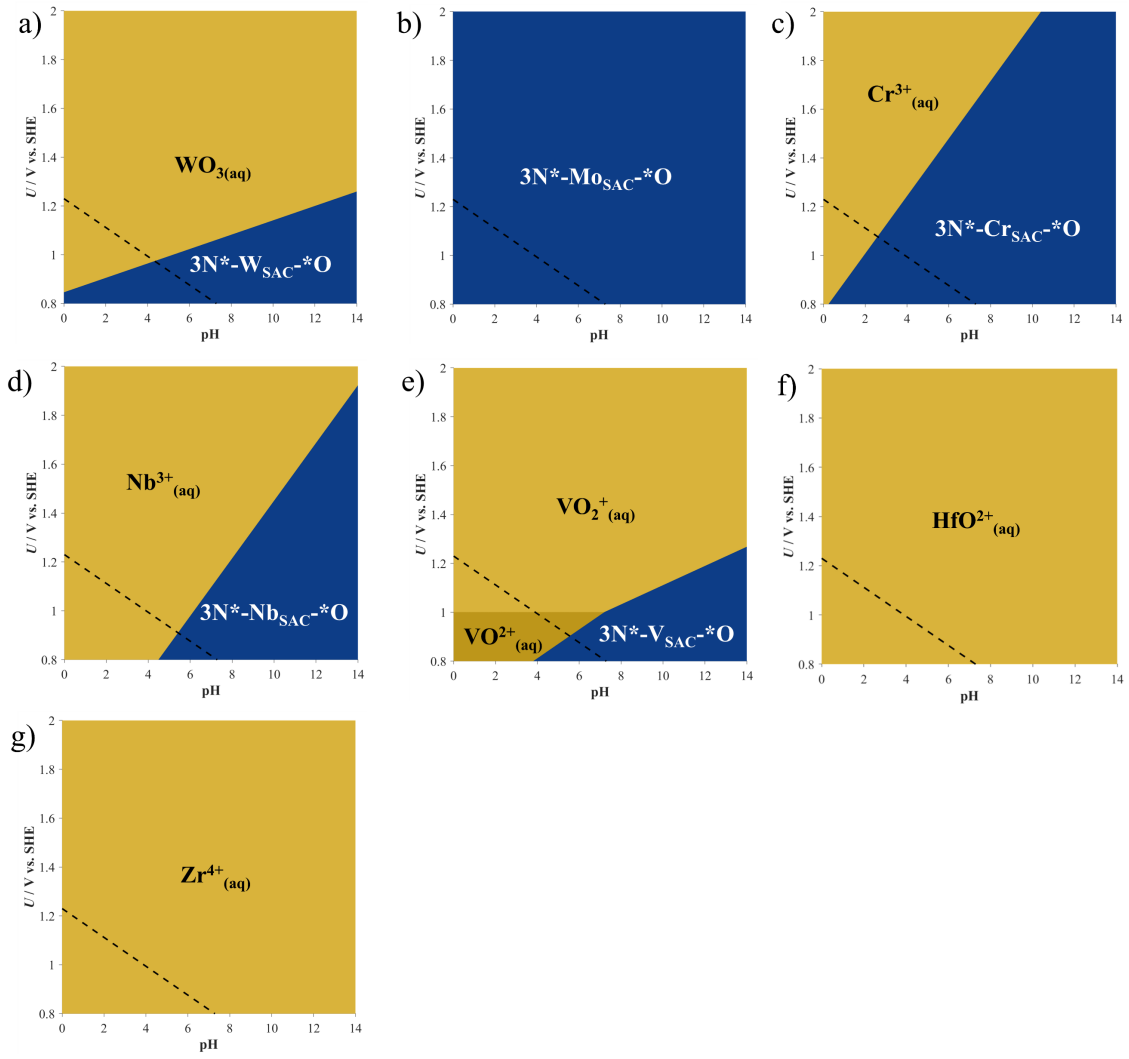

Figure S13. Pourbaix diagrams assessing the thermodynamic stability of SAC-like sites on the MXene basal plane, 3N*-M_{SAC}-*O, of a) W_3N_2O, b) Mo_3N_2O, c) Cr_3N_2O, d) Nb_3N_2O, e) V_3N_2O, f) Hf_3N_2O and g) Zr_3N_2O MXenes in the context of the pre-OER scenario (*cf.* **Figure S1**). The stability of M_{SAC} is referenced to different oxidative ion states resulting from the dissolution of the corresponding metals (*cf.* **Table S4** in the SI). Regions where 3N*-M_{SAC}-*O is thermodynamically stable are colored blue, while a yellow background indicates that metal cations are energetically favored. The black, dashed line indicates the OER equilibrium potential on the SHE scale.

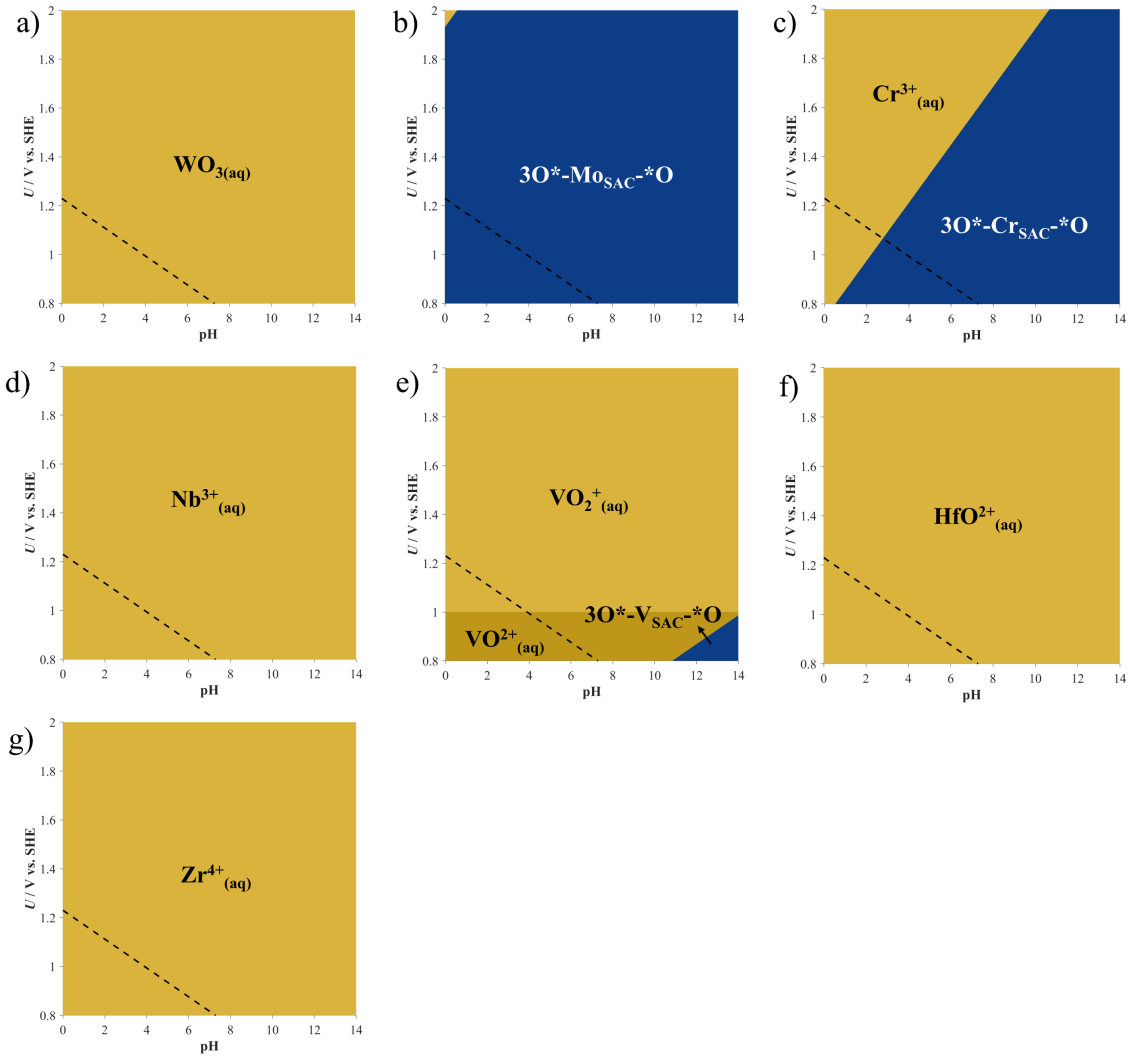

Figure S14. Pourbaix diagrams assessing the thermodynamic stability of SAC-like sites on the MXene basal plane, 3O*-M_{SAC}-*O, of a) W_3N_2O, b) Mo_3N_2O, c) Cr_3N_2O, d) Nb_3N_2O, e) V_3N_2O, f) Hf_3N_2O and g) Zr_3N_2O MXenes in the context of the pre-OER scenario (*cf.* **Figure S1**). The stability of M_{SAC} is referenced to different oxidative ion states resulting from the dissolution of the corresponding metals (*cf.* **Table S4** in the SI). Regions where 3O*-M_{SAC}-*O is thermodynamically stable are colored blue, while a yellow background indicates that metal cations are energetically favored. The black, dashed line indicates the OER equilibrium potential on the SHE scale.

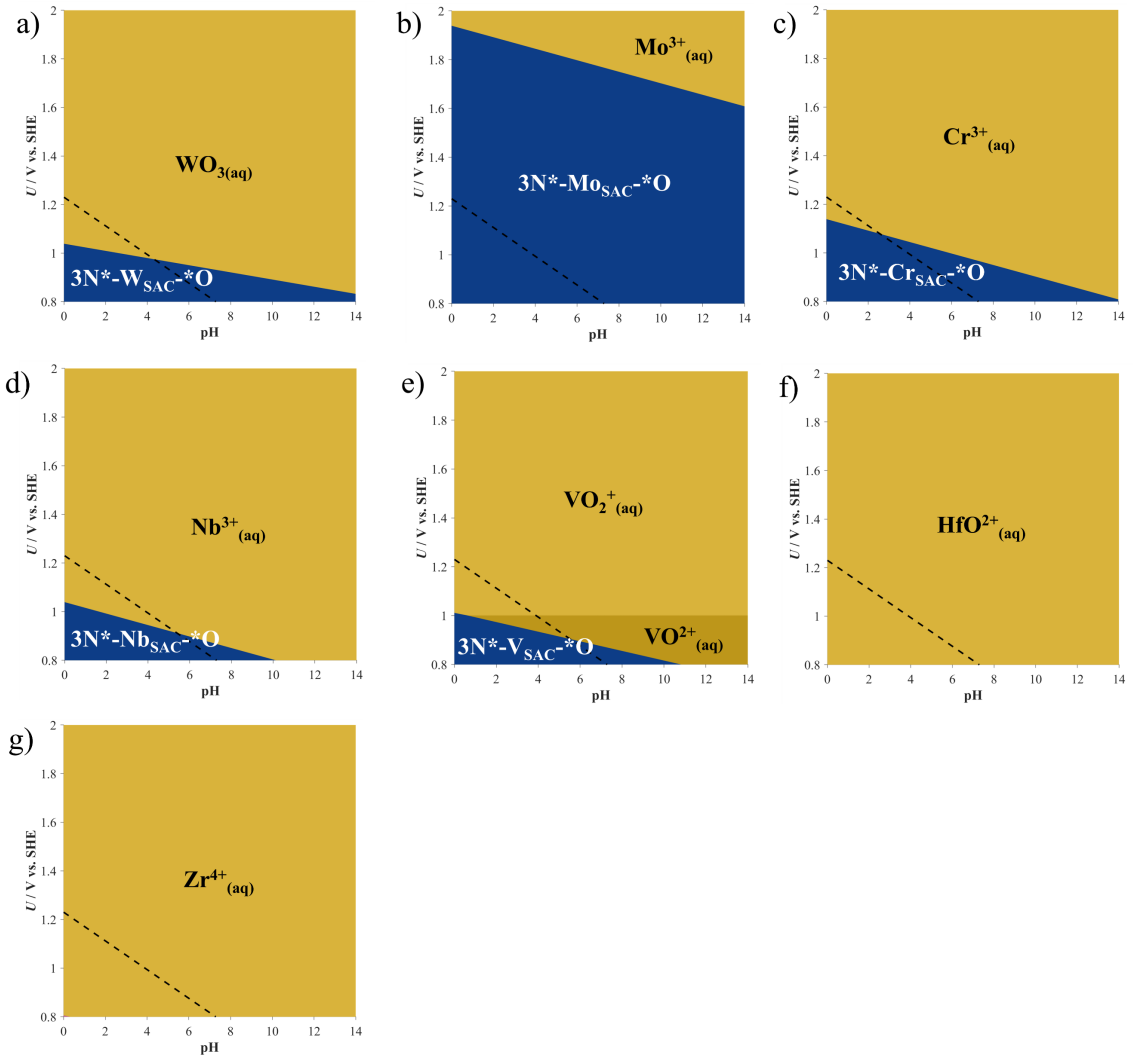

Figure S15. Pourbaix diagrams assessing the thermodynamic stability of SAC-like sites on the MXene basal plane, 3N*-M_{SAC}-*O, of a) W_3N_2O, b) Mo_3N_2O, c) Cr_3N_2O, d) Nb_3N_2O, e) V_3N_2O, f) Hf_3N_2O and g) Zr_3N_2O MXenes in the context of the OER scenario (*cf.* **Figure S2**). The stability of M_{SAC} is referenced to different oxidative ion states resulting from the dissolution of the corresponding metals (*cf.* **Table S4** in the SI). Regions where 3N*-M_{SAC}-*O is thermodynamically stable are colored blue, while a yellow background indicates that metal cations are energetically favored. The black, dashed line indicates the OER equilibrium potential on the SHE scale.

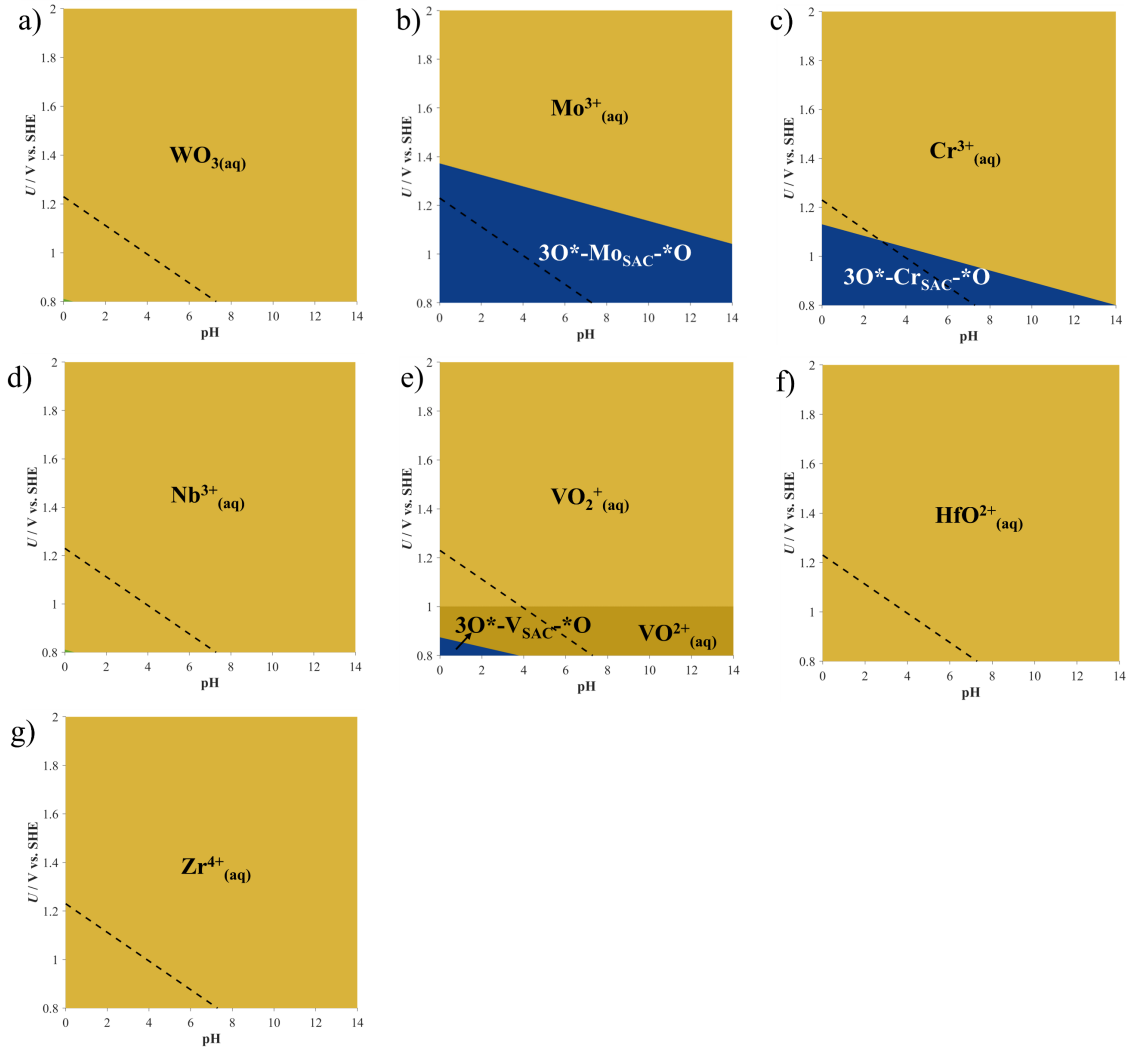

Figure S16. Pourbaix diagrams assessing the thermodynamic stability of SAC-like sites on the MXene basal plane, 3O*-M_{SAC}-*O, of a) W_3N_2O, b) Mo_3N_2O, c) Cr_3N_2O, d) Nb_3N_2O, e) V_3N_2O, f) Hf_3N_2O and g) Zr_3N_2O MXenes in the context of the OER scenario (*cf.* **Figure S2**). The stability of M_{SAC} is referenced to different oxidative ion states resulting from the dissolution of the corresponding metals (*cf.* **Table S4** in the SI). Regions where 3O*-M_{SAC}-*O is thermodynamically stable are colored blue, while a yellow background indicates that metal cations are energetically favored. The black, dashed line indicates the OER equilibrium potential on the SHE scale.

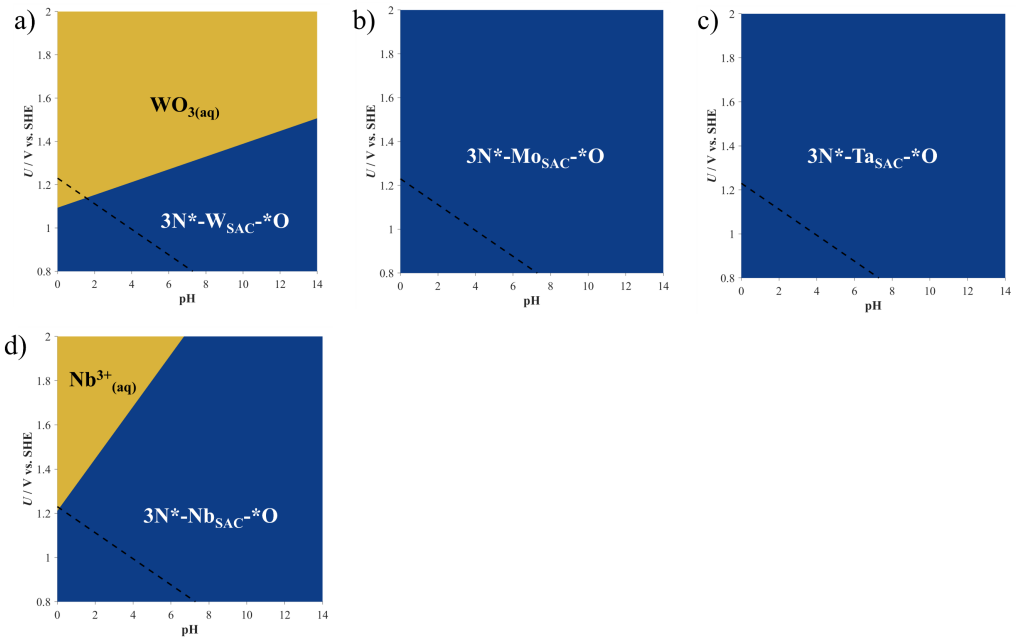

Figure S17. Pourbaix diagrams assessing the thermodynamic stability of SAC-like sites on the MXene basal plane, 3N*-M_{SAC}-*O, of a) W_4C_3O, b) Mo_4C_3O, c) Ta_4C_3O and d) Nb_4C_3O MXenes in the context of the pre-OER scenario (*cf.* **Figure S1**). The stability of M_{SAC} is referenced to different oxidative ion states resulting from the dissolution of the corresponding metals (*cf.* **Table S4** in the SI). Regions where 3N*-M_{SAC}-*O is thermodynamically stable are colored blue, while a yellow background indicates that metal cations are energetically favored. The black, dashed line indicates the OER equilibrium potential on the SHE scale.

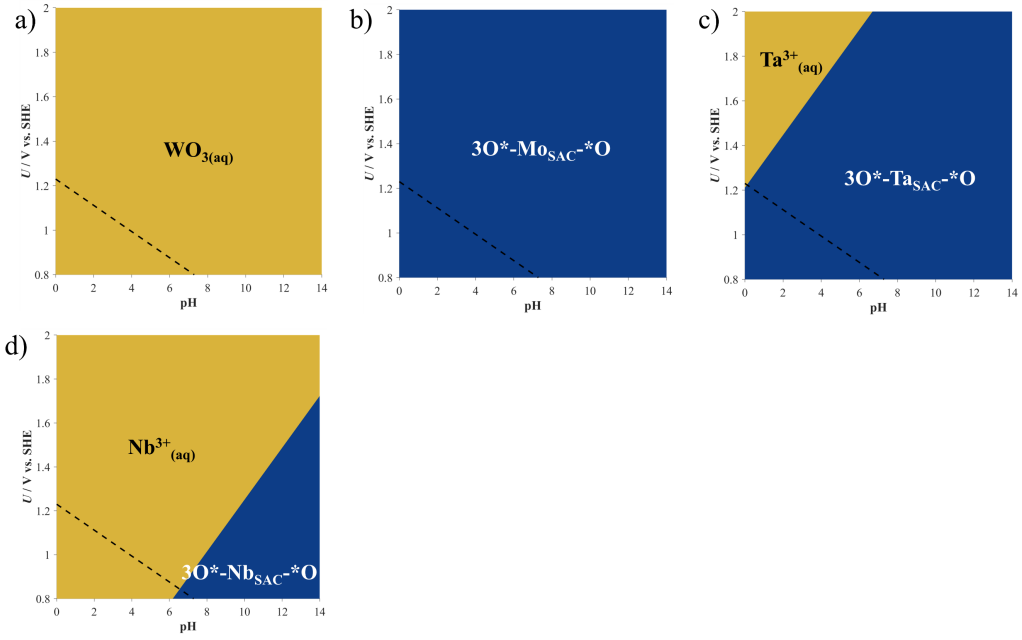

Figure S18. Pourbaix diagrams assessing the thermodynamic stability of SAC-like sites on the MXene basal plane, 3O*-M_{SAC}-*O, of a) W_4C_3O, b) Mo_4C_3O, c) Ta_4C_3O and d) Nb_4C_3O MXenes in the context of the pre-OER scenario (*cf.* **Figure S1**). The stability of M_{SAC} is referenced to different oxidative ion states resulting from the dissolution of the corresponding metals (*cf.* **Table S4** in the SI). Regions where 3O*-M_{SAC}-*O is thermodynamically stable are colored blue, while a yellow background indicates that metal cations are energetically favored. The black, dashed line indicates the OER equilibrium potential on the SHE scale.

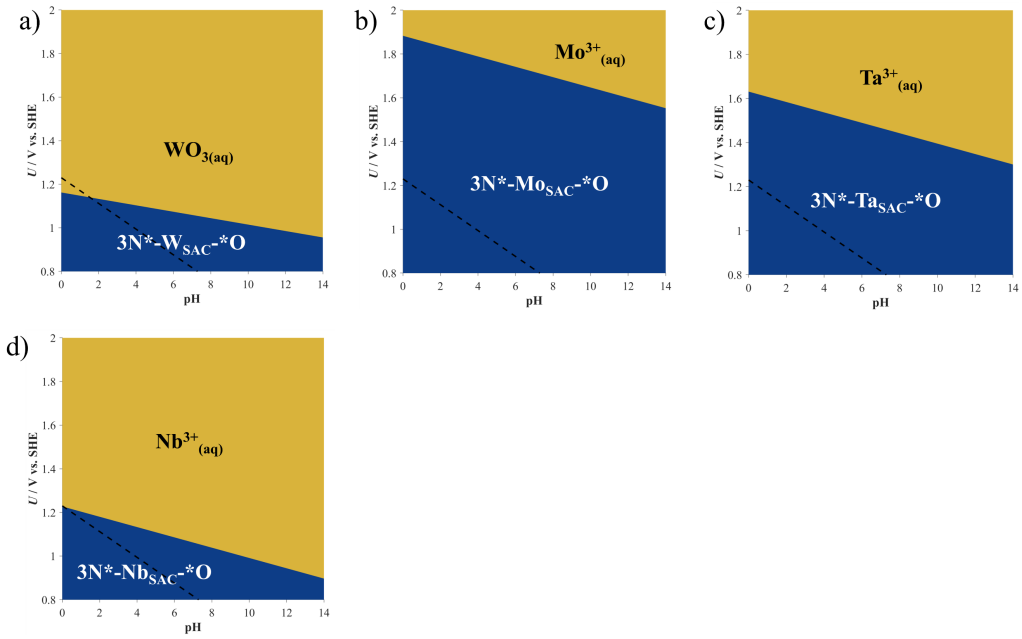

Figure S19. Pourbaix diagrams assessing the thermodynamic stability of SAC-like sites on the MXene basal plane, 3N*-M_{SAC}-*O, of a) W_4C_3O, b) Mo_4C_3O, c) Ta_4C_3O and d) Nb_4C_3O MXenes in the context of the OER scenario (*cf.* **Figure S2**). The stability of M_{SAC} is referenced to different oxidative ion states resulting from the dissolution of the corresponding metals (*cf.* **Table S4** in the SI). Regions where 3N*-M_{SAC}-*O is thermodynamically stable are colored blue, while a yellow background indicates that metal cations are energetically favored. The black, dashed line indicates the OER equilibrium potential on the SHE scale.

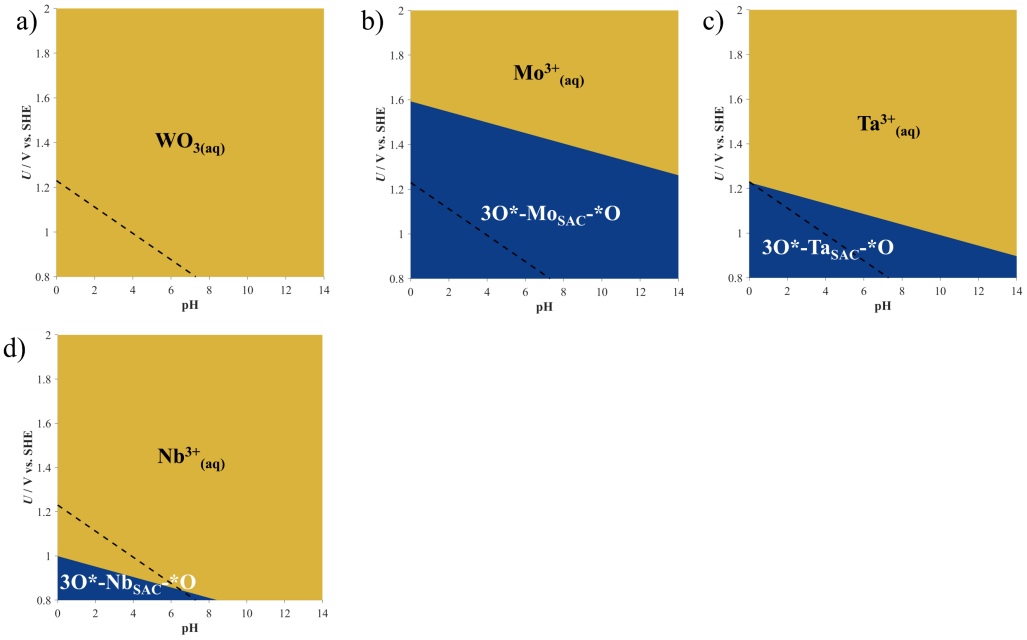

Figure S20. Pourbaix diagrams assessing the thermodynamic stability of SAC-like sites on the MXene basal plane, 3O*-M_{SAC}-*O, of a) W_4C_3O, b) Mo_4C_3O, c) Ta_4C_3O and d) Nb_4C_3O MXenes in the context of the OER scenario (*cf.* **Figure S2**). The stability of M_{SAC} is referenced to different oxidative ion states resulting from the dissolution of the corresponding metals (*cf.* **Table S4** in the SI). Regions where 3O*-M_{SAC}-*O is thermodynamically stable are colored blue, while a yellow background indicates that metal

cations are energetically favored. The black, dashed line indicates the OER equilibrium potential on the SHE scale.

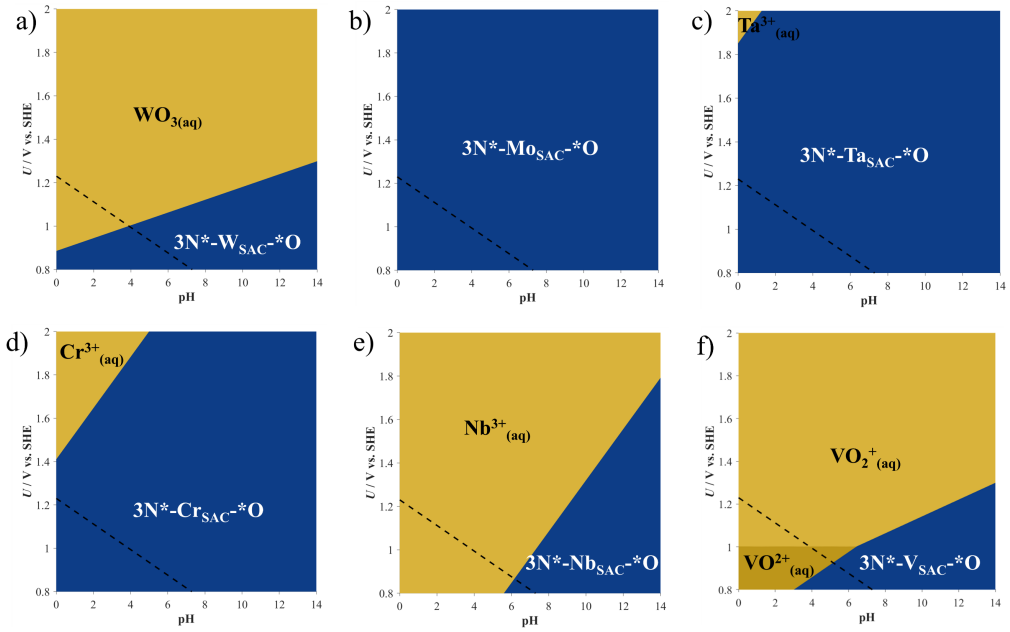

Figure S21. Pourbaix diagrams assessing the thermodynamic stability of SAC-like sites on the MXene basal plane, 3N*-M_{SAC}-*O, of a) W_4N_3O, b) Mo_4N_3O, c) Ta_4N_3O, d) Cr_4N_3O, e) Nb_4N_3O and f) V_4N_3O MXenes in the context of the pre-OER scenario (*cf.* **Figure S1**). The stability of M_{SAC} is referenced to different oxidative ion states resulting from the dissolution of the corresponding metals (*cf.* **Table S4** in the SI). Regions where 3N*-M_{SAC}-*O is thermodynamically stable are colored blue, while a yellow background indicates that metal cations are energetically favored. The black, dashed line indicates the OER equilibrium potential on the SHE scale.

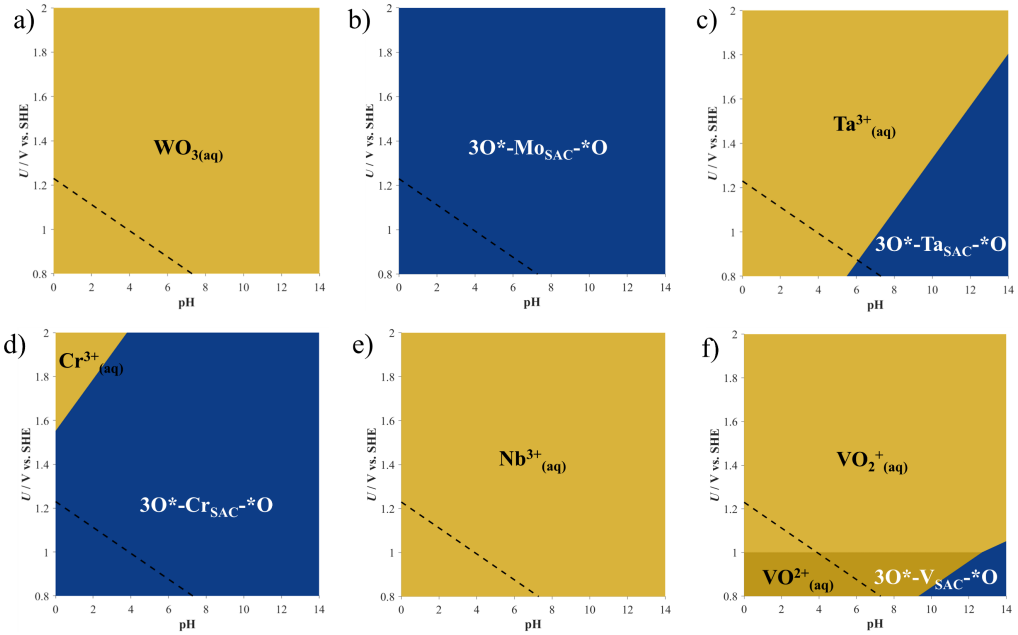

Figure S22. Pourbaix diagrams assessing the thermodynamic stability of SAC-like sites on the MXene basal plane, 3O*-M_{SAC}-*O, of a) W_4N_3O, b) Mo_4N_3O, c) Ta_4N_3O, d) Cr_4N_3O, e) Nb_4N_3O and f) V_4N_3O MXenes in the context of the pre-OER scenario (*cf.* **Figure S1**). The stability of M_{SAC} is referenced to different oxidative ion states resulting from the dissolution of the corresponding metals (*cf.* **Table S4** in

the SI). Regions where 3O*-M_{SAC}-*O is thermodynamically stable are colored blue, while a yellow background indicates that metal cations are energetically favored. The black, dashed line indicates the OER equilibrium potential on the SHE scale.

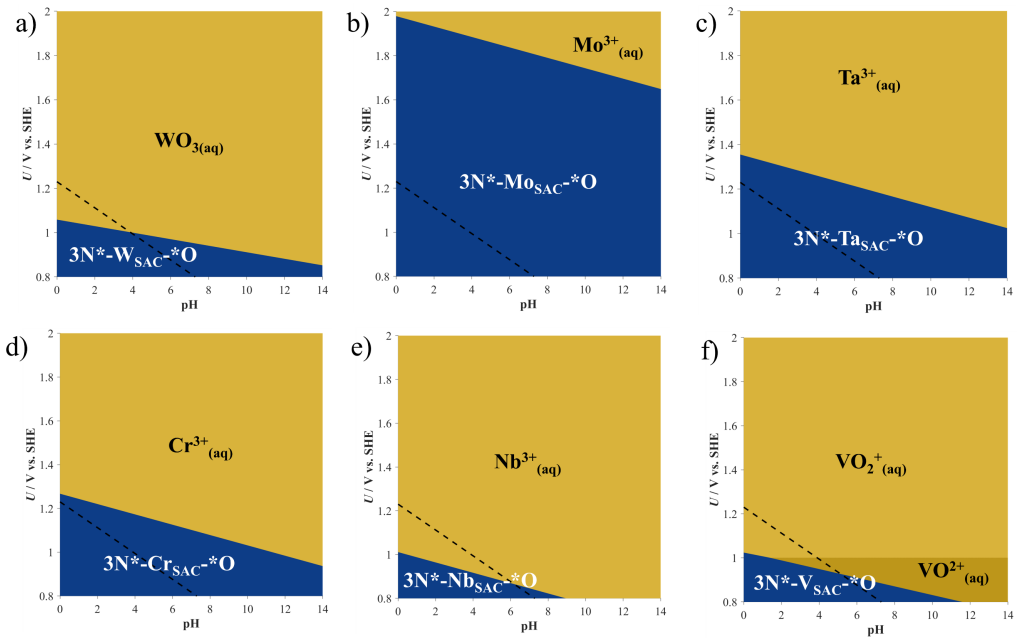

Figure S23. Pourbaix diagrams assessing the thermodynamic stability of SAC-like sites on the MXene basal plane, 3N*-M_{SAC}-*O, of a) W_4N_3O, b) Mo_4N_3O, c) Ta_4N_3O, d) Cr_4N_3O, e) Nb_4N_3O and f) V_4N_3O MXenes in the context of the OER scenario (*cf.* **Figure S2**). The stability of M_{SAC} is referenced to different oxidative ion states resulting from the dissolution of the corresponding metals (*cf.* **Table S4** in the SI). Regions where 3N*-M_{SAC}-*O is thermodynamically stable are colored blue, while a yellow background indicates that metal cations are energetically favored. The black, dashed line indicates the OER equilibrium potential on the SHE scale.

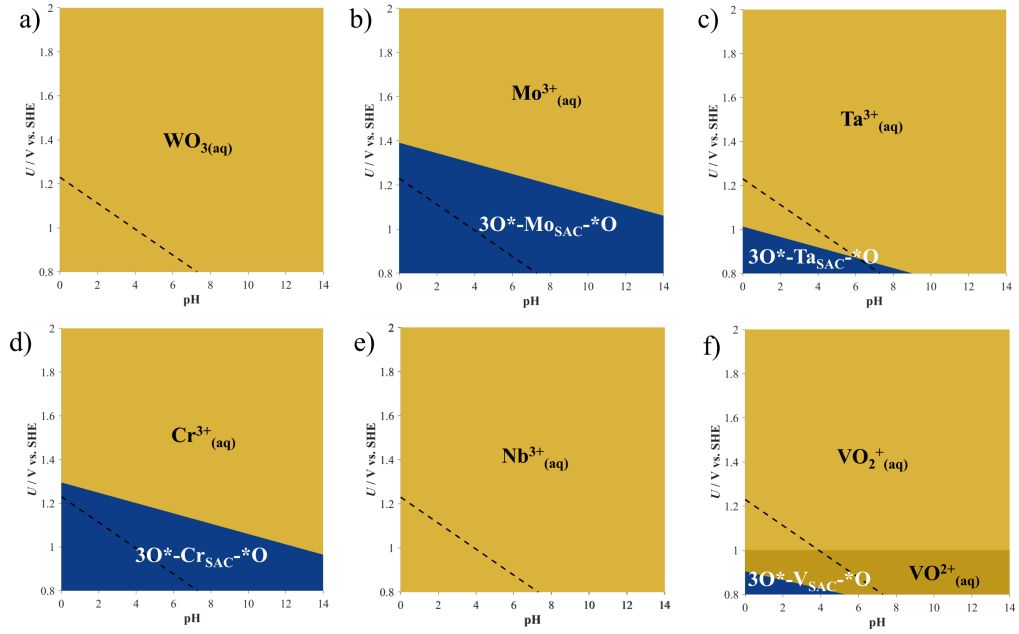

Figure S24. Pourbaix diagrams assessing the thermodynamic stability of SAC-like sites on the MXene basal plane, 3O*-M_{SAC}-*O, of a) W_4N_3O, b) Mo_4N_3O, c) Ta_4N_3O, d) Cr_4N_3O, e) Nb_4N_3O and f) V_4N_3O MXenes in the context of the OER scenario (*cf.* **Figure S2**). The stability of M_{SAC} is referenced to different

oxidative ion states resulting from the dissolution of the corresponding metals (*cf.* **Table S4** in the SI). Regions where 3O*-M_{SAC}-*O is thermodynamically stable are colored blue, while a yellow background indicates that metal cations are energetically favored. The black, dashed line indicates the OER equilibrium potential on the SHE scale.

Reference

1. Meng, L., Viñes, F., Illas, F. & Exner, K. S. Stability of single-atom centers of MXenes under anodic polarization conditions. *J. Phys. Chem. C* **129**, 9589–9601 (2025).